Absolute total ionization cross sections of uracil ($C_4H_4N_2O_2$) in collisions with MeV energy highly charged carbon, oxygen and fluorine ions

2013 J. Phys. B: At. Mol. Opt. Phys. 46 185201

(http://iopscience.iop.org/0953-4075/46/18/185201)

J. Phys. B: At. Mol. Opt. Phys. **46** (2013) 185201 (8pp) doi:10.1088/0953-4075/46/18/185201

Absolute total ionization cross sections of uracil ($C_4H_4N_2O_2$) in collisions with MeV energy highly charged carbon, oxygen and fluorine ions

A N Agnihotri[1], S Kasthurirangan[2], S Nandi[1], A Kumar[3], C Champion[4], H Lekadir[4], J Hanssen[4], P F Weck[5], M E Galassi[6], R D Rivarola[6], O Fojón[6] and L C Tribedi[1]

[1] Tata Institute of Fundamental Research, Colaba, Mumbai 400005, India
[2] Institute of Chemical Technology, Matunga, Mumbai 400019, India
[3] Nuclear Physics Division, BARC, Trombay, Mumbai 400085, India
[4] LPMC, Universite Paul Verlaine-Metz, France
[5] Department of Chemistry, University of Nevada, Las Vegas, NV 89154, USA
[6] Instituto de Física Rosario, Rosario, Argentina

E-mail: lokesh@tifr.res.in

Received 3 February 2013, in final form 6 August 2013
Published 5 September 2013
Online at stacks.iop.org/JPhysB/46/185201

Abstract
Ionization and fragmentation of uracil molecules ($C_4H_4N_2O_2$, $m = 112$ amu) in collisions with fast highly charged C, O and F ions have been investigated using a time-of-flight mass spectrometer. The measurement of total ionization cross sections (TCS) is reported for different charge states (q), such as F^{q+} with $q = 5$–8; O^{q+} with $q = 5,7$; C^{q+} with $q = 5$ and 6. These studies reveal a $(q/v)^{\sim 1.5}$ dependence of TCS, in contrast, to the well-known q^2-dependence in ion–atom collisions. Scaling properties of the TCS with projectile energy and charge states are obtained. The experimental results for TCS measurements are compared with the theoretical calculations performed within classical and quantum mechanical frameworks. The trends in energy dependence of the TCSs is qualitatively well reproduced by the different models and more specifically by the classical description, which provides the best agreement with measurements.

(Some figures may appear in colour only in the online journal)

1. Introduction

Ionization is one of the important processes in atomic collisions with photons, electrons and ions. For collisions involving MeV energy fast heavy ions, ionization plays a dominant role over other processes, such as electron capture [1]. In fast-ion collisions with atoms, simple first-order perturbative models do not reproduce the details of the ionization mechanism. One needs to use the models which include the distortion of the target wavefunction of both the initial and final states. It has been shown in the past that the CDW–EIS (continuum distorted wave–eikonal initial state) approximation is suitable to explain many of the ionization features, such as the two-centre effect, binary encounter and cusp electron peak in ion–atom collisions [2–8].

In the case of large molecules or other mesoscopic systems, additional complications arise. A determination of the suitable wavefunction of the initial state for such many-body molecules is one of the most challenging tasks. Although there is a lack of experimental data, as well as *ab initio* theoretical support, rapid progress on the theoretical and experimental front has been noticed in the last few years. In particular, the experimental investigations on charge particle collisions with the DNA/RNA base molecules have attracted a great deal of attention. Apart from their importance in collision physics, these studies find applications in many fields, such

as radiobiology and hadron therapy. Indeed, nowadays it is well established that the lethal events for living cells can be attributed to the complex clustered damages coupling DNA base lesions with the single and double strand breaks. Since it is a well-established fact that the ionization process is primarily responsible for the double strand breaks, a detailed knowledge of the heavy ion-induced ionization mechanism is of importance for radiobiologists. Accurate ionization cross sections of biomolecules are proved to be useful input for the Monte Carlo type of numerical simulations devoted to the modelling of radiation-induced cellular damages [9, 10].

The investigation of ion-induced collisions, particularly for carbon ions, are crucial in modelling the cell-damage processes, since the GeV energy C ions are commonly used for cancer treatments in major high-energy heavy-ion accelerator facilities. In heavy-ion therapy, the energy loss of swift ions while penetrating the body is continuous and exhibits a maximum in an energy range known as the Bragg-peak region. Therefore, the study of the energetic ion impact on nucleobases over a wide energy range, provides some necessary inputs to model the degree of radiation damage. However, the experimental measurements on such single molecular biological systems remain scarce. The investigations of fast ion-induced ionization of such molecules are only rarely reported in the literature. The low-energy proton-induced ionization of uracil was recently investigated by a few groups [11–13]. In this context, Tabet *et al* [14] measured the ionization and fragmentation of uracil under the impact of keV energy protons and derived the branching ratios of the capture and ionization processes. Total ionization cross sections of uracil in collisions with keV–MeV energy ions were mainly limited to He-like ions [15]. Additionally, the measurements of ionization and fragmentation of isolated nucleobases were also reported by de Vries *et al* [16], Brédy *et al* [17] and others [18–21]. The study of uracil ionization, as presented in this work, can provide a benchmark study for the fast-ion collisions with the other DNA base molecules.

On the theoretical side, ion collisions with DNA components have rarely been studied. For example, one may refer to the model based on the classical trajectory Monte Carlo (CTMC) description provided by Bacchus-Montabonel *et al* [22]. Then Champion and co-workers [23, 24] proposed a modified classical approach in which the usual CTMC model was coupled with a classical over-barrier (COB) criteria. A quantum mechanical approach was also developed where the differential and total ionization cross sections were calculated within the first Born framework for proton impact on DNA bases [25, 26]. Finally, let us note that Champion *et al* have recently proposed a CDW–EIS description of the ionization and capture process [27, 28].

In the present work, we focus on the measurements of the absolute total ionization cross sections and their comparisons with theoretical predictions using the CTMC–COB, CDW–EIS [29, 30] and CB1 (first Born model with correct boundary condition) models [31]. The fundamental state of uracil was described by the restricted Hartree–Fock method with geometry optimization [27] within the particular orbital energies obtained with the Gaussian-09 software at the RHF-21G level [32]. Finally, each molecular orbital of uracil is then described by a linear combination of atomic orbitals.

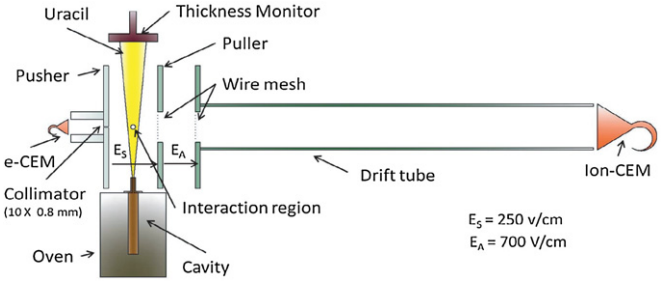

Figure 1. Schematic diagram of the ToF setup.

2. Details of the experiment

2.1. Experimental setup

The experimental setup consists of a vacuum chamber with a Wiley–McLaren type of recoil-ion time-of-flight (ToF) spectrometer. Uracil powder was heated in an oven to produce the target in vapour form. The schematic diagram of the spectrometer with an oven and detectors is shown in figure 1. In the chamber, the collimated ion beams cross the gaseous target of uracil between the pusher and puller plates of the spectrometer. In figure 1, the direction of the ion beam is chosen to be perpendicular to the plane of the paper. The pressure in the scattering chamber was better than 4×10^{-7} Torr throughout the experiment. Details of the target preparation are given in the next section. The electrons and ions, produced in the ionization process, move in opposite directions due to the applied electric field (E_S = 250 V cm^{-1}). The electrons are collected by a channel electron multiplier (indicated as the e-CEM in figure 1). A slit (10 × 0.8 mm) was placed in front of the e-CEM to reduce the excessive count rate. The ions are further accelerated (E_A = 700 V cm^{-1}) and collected by the ion CEM after passing the field free region of length ∼23 cm. The front voltage of the ion CEM was −4000 volts. The electron and the ion-CEM output signals are given to a constant fraction discriminator (CFD). The CFD outputs of the electron and ion signals were used, respectively, as the START and STOP signals of a time-to-amplitude converter (TAC). A current integrator was used to monitor the ion current. The output of the TAC and the current integrator is given to a CAMAC compatible ADC and a scaler, respectively.

The experiments were carried out using the energetic C, O and F ions (v = 7 to 15 au) produced in the BARC-TIFR 14 MV tandem Pelletron accelerator facility at TIFR. First, the energy and charge state selected ion beams were obtained from the accelerator and then the ions were passed through a post accelerator carbon foil stripper to produce the higher charge states of the ions. A switching magnet was used to select the charge states of interest.

2.2. Target preparation: control and monitoring

To prepare the gaseous target of uracil, the commercially available uracil powder (99% pure, Sigma-Aldrich) was heated

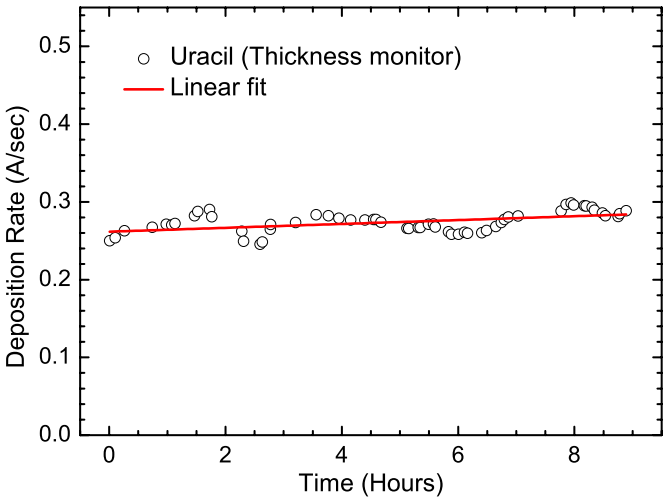

Figure 2. Plot of uracil deposition rate versus time.

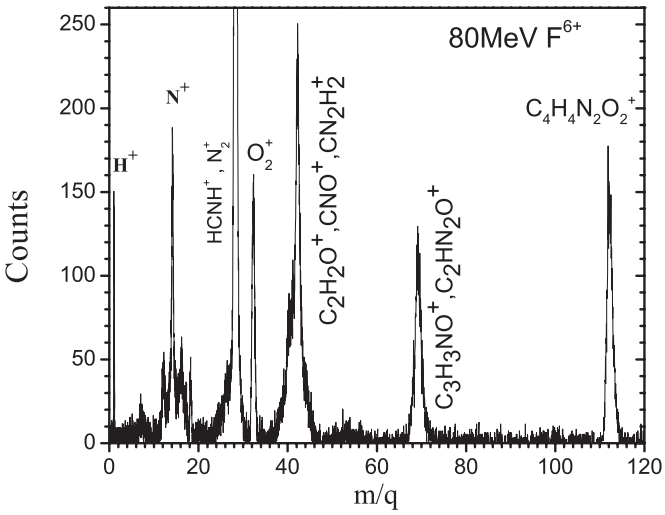

Figure 3. Typical ToF spectrum of uracil.

in an oven. A quartz container filled with the powder was kept in a cavity in the oven. The cavity was heated resistively which in turn heats the quartz container and the uracil comes out through a nozzle, forming an effusive jet of molecules. Maintaining uniform flow of molecules was crucial. The molecules were heated very slowly and about eight to ten hours were necessary to reach the appropriate target density. The oven temperature was kept at about 160° C which was sufficient to produce enough vapour density in the interaction region. The temperature was kept well below the dissociation temperature of the molecule to avoid any thermal breakup.

To monitor the flow of molecules throughout the experiment, a quartz crystal thickness monitor [33] was suitably mounted. The monitor uses a Cr/Au 6 MHZ crystal on which the uracil layer is deposited. The monitor displays the thickness of the deposited layer (kÅ) and also the rate of deposition. Figure 2 shows a plot of the deposition rate versus the time over an interval of ∼10 h. Variation of the deposition rate was found to be within 5–10%.

3. Results and discussions

3.1. Time-of-flight spectra and measurement of TCS

Figure 3 displays the typical ToF spectrum of uracil in collisions with the F^{6+} ions of energy 80 MeV. The spectrum mainly consists of the peaks corresponding to the ions of m/q = 112 ($C_4H_4N_2O_2^+$, denoted by Ur^+ for the rest of the paper), 69 ($C_3H_3NO^+$,$C_2HN_2O^+$), 42 ($C_2H_2O^+$,CNO^+,$CN_2H_2^+$), 28 ($HCNH^+$,CO^+) and 1 (H^+). The yield of the mass 42 fragment includes ions of masses from 39 to 43 which could not be resolved ($\Delta m/m \sim 0.025$). The ToF spectra of uracil in collisions with the C and O ions also show similar mass fragments. The mass fragment 69 ($C_3H_3NO^+$) can be formed by the loss of a HCNO fragment (m/q = 43) from the parent cation i.e., Ur^+. Further fragmentation of the mass 69 component can lead to the lower mass ions. Possible and energetically favourable structures of the fragments have been reported by Jochims *et al* [34]. The strongest peak is observed for the fragment with m/q = 42. Fragmentation patterns observed in the photoionization and the ion/electron-impact ionization of the uracil molecule [34–38] are quite similar. The peak corresponding to the doubly ionized uracil was not observed at any projectile energy and charge state.

The total ionization cross section was obtained by integrating the ToF spectra over all (parent + fragment) of the ion peaks after the background subtraction. This definition of TCS, which implicitly includes the multiple ionization and transfer ionization (TI) and excludes the capture process, can be termed as the total electron emission cross section. However, the contribution of TI is small in this velocity range [39, 40], therefore this definition of TCS is in accordance with that in [41].

3.2. Background subtraction

The peak at m/q = 28 contains $HCNH^+$ and CO^+ coming from uracil breakup. In addition, it also contains the recoil-ions of N_2^+ arising from the background gas. To estimate the contribution of the background, the ToF spectrum was taken without the target at several energies. The ratio of the yields of N_2^+ to that of O_2^+ was plotted as a function of the energy. The ratio was found to be fairly constant with a value of ∼4.0. Since the O_2^+ contribution comes only from the background, this ratio was used to calculate the contribution of the N_2^+ yields in the m/q = 28 peak. The total yield of the fragments $HCNH^+$ and CO^+ was then obtained by subtracting the background from the total peak area. The N_2^+ yield was found to be about ∼70% of this peak.

3.3. Absolute normalization of TCS

The absolute normalization of the cross sections, using first principles, is a very difficult task. An accurate estimation of the target density and the jet profile in the interaction region is required. This requires the vapour pressure which needs the accurate temperature information of the molecules inside the cavity. Apart from this, the detection efficiency for different mass fragments should also be known. To avoid these difficulties, a novel technique for the normalization was

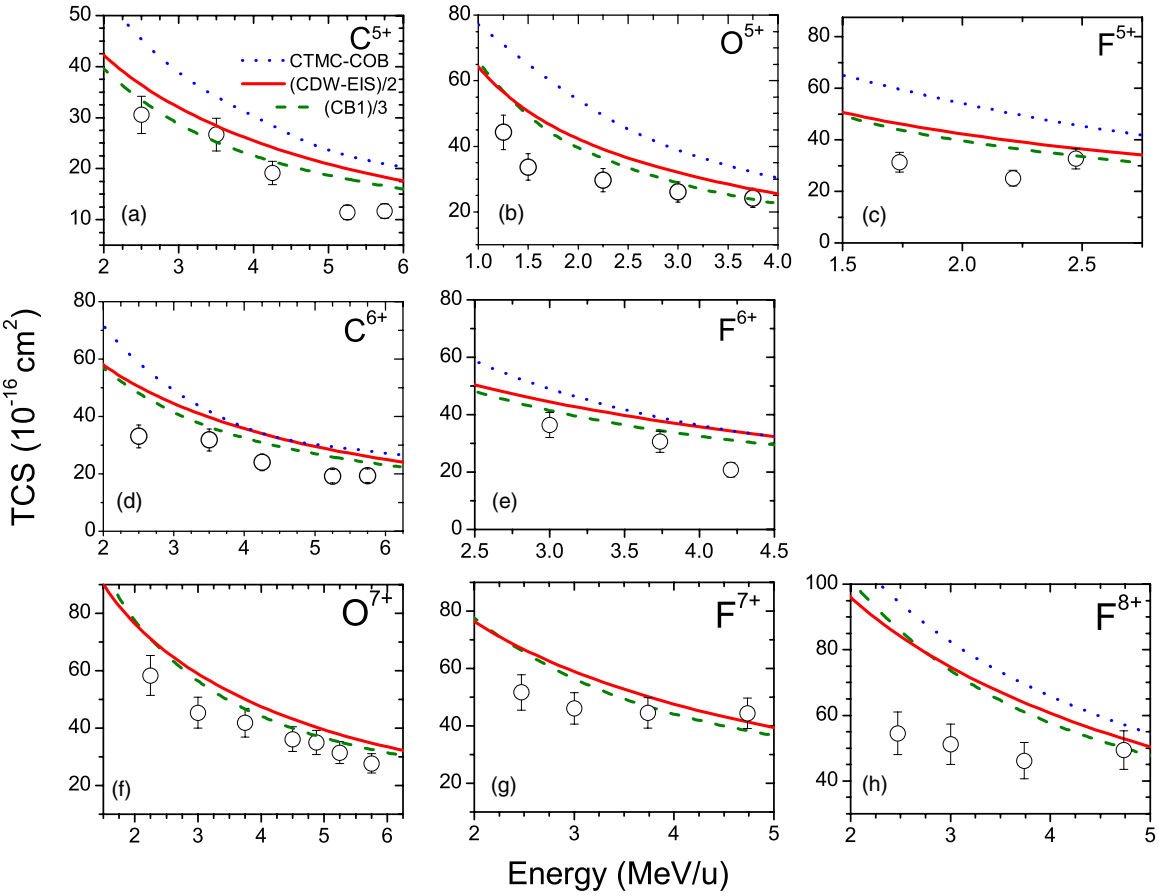

Figure 4. Absolute TCS (fragmentation + ionization) of uracil in collisions with C, O and F ions.

adopted. Since the target density and other geometrical factors are the same for all the energies studied, the knowledge of the absolute cross sections at one energy is sufficient to normalize the data for all other energies. Therefore, first, in a separate experiment, the absolute TCS (σ_{abs})of the ionization of uracil in collisions with 42 MeV C^{6+} ions was measured by detecting all of the electrons emitted with different energies and in different angles using an electrostatic hemispherical analyser setup. Then, the normalization factor (N) was obtained by taking the ratio of σ_{abs} (obtained from the electron spectroscopy experiment) to the relative TCS (σ_{rel}) which was obtained by the present ToF based experiment at the same energy i.e., 42 MeV C^{6+}. This factor N ($\frac{\sigma_{abs}}{\sigma_{rel}}$) was used to put the entire TCS data obtained into the ToF experiments with the projectiles with different energies on an absolute scale. The details of the normalization procedure can be found in the appendix below.

3.4. Projectile energy dependence of TCS

Figure 4 shows the absolute TCS data in collisions with the C($q = 5, 6$), O ($q = 5, 7$) and F ($q = 5, 6, 7, 8$) projectile ions. The total cross sections were plotted as a function of the projectile energy (∼1–6 MeV/u). The relative errors are about ∼12% which are shown on the data points. This error arises mainly from the deposition rate fluctuation as mentioned earlier in section 2.2. However, the total absolute error was estimated to be ∼23% which includes the relative error and the error from the normalization procedure. The panels in figure 4 are arranged according to the charge states of the projectiles. This is done for better comparisons among the projectiles with the same q but with different atomic number (Z). For most of the projectiles, the cross sections fall sharply as the projectile energy increases. This behaviour is similar to the case of a typical ion–atom collision process. Since the typical velocity of the projectile ions, as studied here, is much higher than the orbital velocity of the target electrons, the cross sections fall sharply with the projectile energy. The experimental data are compared with the CTMC–COB (for $q = 5, 6, 8$), the CB1 and the CDW–EIS calculations. In figure 4, CDW–EIS and CB1 calculations are divided by a factor of two and three, respectively, to show the qualitative agreement with the measured data. The comparison shows a qualitative agreement between experimental data and theory. The sharp fall of the cross sections with increasing projectile energy is reproduced in most of the cases except for the data obtained with the F^{8+} ions. The CTMC–COB calculation, however, falls closer to the data as compared to the other models. Given the complication of the collision system the quantitative as well as qualitative agreements with the models are encouraging.

3.5. Projectile charge state (q) dependence of TCS

The ionization and fragmentation processes and the energy loss of the projectile depend on the perturbation strength ($\frac{q}{v}$)

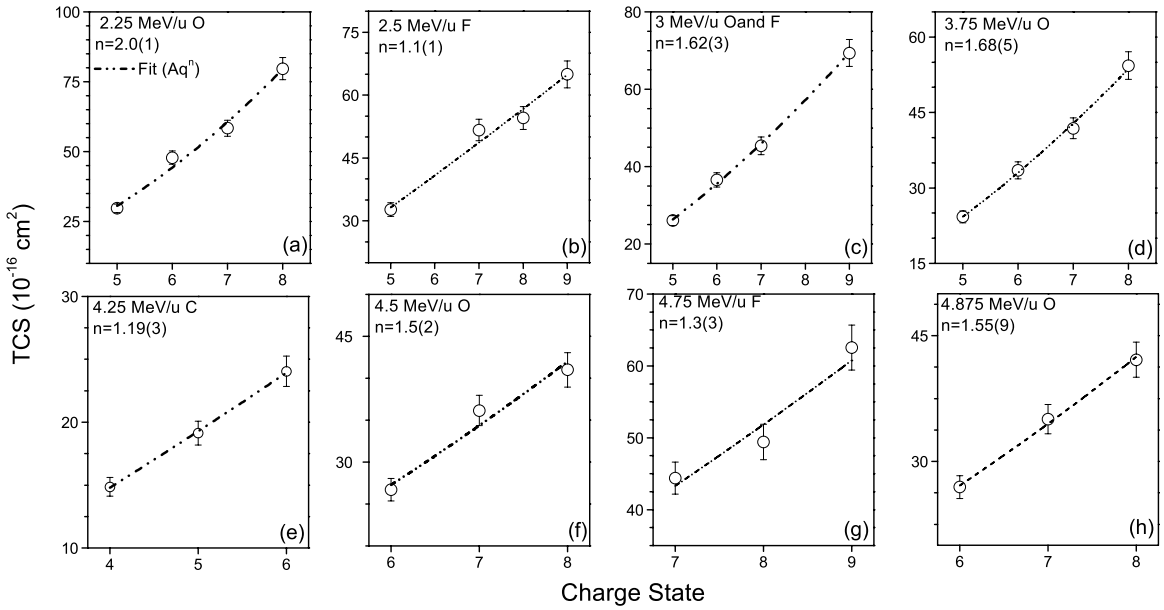

Figure 5. Charge state dependence of total ionization cross sections. Numbers in the parenthesis are the errors in the last digit of the *n* values.

of the collision. The charge state of the projectile can be varied in order to vary the perturbation strength in a collision keeping the velocity of the ions constant. A quadratic q-dependence of the single ionization of atoms in fast collisions is well-known from the experiments and is well predicted by the first-order perturbative models. However, in the present collision system involving such large molecules, it is not obvious whether such a q^2-dependence can be used. To study the effect of the dressed projectiles on the ionization cross sections, the ToF spectra for different q for all the projectiles (C, O and F) were recorded.

Figure 5 shows the q-dependence of the TCS in collisions with all three projectiles having energies between 2.25 MeV/u to 4.875 MeV/u. The q-dependence seems to be deviating from the expected quadratic behaviour according to the first-order theories employing an independent electron model[42, 43]. The experimental data were fitted to a power law (Aq^n) (shown in figure 5(a), (c) and (e)) and the *n* values were found to be varying from a maximum value of 2.0(1) to a minimum of 1.1(1) with the average value ∼1.5. The *n* values for each case are shown in the plots. Numbers in the parenthesis are the errors in the last digit of the *n* values obtained. The deviation from the q^2-dependence was also observed in the case of collisions involving other many-body systems, such as fullerenes [44, 45], in which case the linear q-dependence was observed. A deviation from q^2-dependence in the case of lower energy collisions (than present energies) have also been reported in the past for He [46, 47] and also for Ne and Ar atoms [39, 48]. In the case of multi-electronic targets, such as Ne and Ar atoms, the reason for such deviation is attributed to the large ionization probabilities [39].

3.6. Scaling of cross sections with q and Eat high energies

Since the experimental data on such biologically significant molecules are not abundant, it is therefore useful if one can establish a scaling property of the cross sections with the projectile charge state and energy. Since the TCS follows $\sim q^{3/2}$-dependence as discussed above, the cross sections for all the projectiles were scaled accordingly and plotted in figure 6. Figure 6(a), shows the TCS_q i.e. TCS divided by $q^{3/2}$. It can be seen that the data for different projectiles fall in a band. The red dotted line was plotted following a $1/E^m$ (with $m = 0.75$) dependence (see below).

The charge state scaled TCSs were then scaled again with $1/E^m$ to give $\mathrm{TCS}_q^E = \mathrm{TCS}_q E^m$. The best values for *m* were found to be $0.75(\pm 0.05)$. The results of the scaling of the TCS for $m = 0.75$ are shown in figure 6(b). It is clear that the appropriately scaled quantity TCS_q^E is independent of *E* and *q*. It is, thereby, easy to see that TCS varies as $(q/v)^{3/2}$. The red dotted lines in these two plots are to guide the eyes and the vertical lines on both ends represent a tentative scale of 20% of the value which includes most of the data points, i.e., roughly quantifying the scattering in the data. Such scaling can be useful for the modelling of the radiation damage-induced by heavy ions. The same scaling procedure can also be used for the different fragment ions since the yields of the fragments follow similar trends when plotted against the projectile energy (see the next section for details).

3.7. Energy dependence of partial cross sections of the fragments and their ratio with TCS

The charged fragments created in the collisions are also of great interest, particularly, in the context of radiation damage in hadron therapy. The mass distributions provide an important input for modelling the damage processes, besides its well-known importance for the collision mechanism involving large molecules. In the present study the fragmentation distributions have also been investigated.

Figures 7(a) and (b) show the relative cross sections for the major fragments produced in the collisions along with the singly ionized uracil ions for two different projectiles i.e.

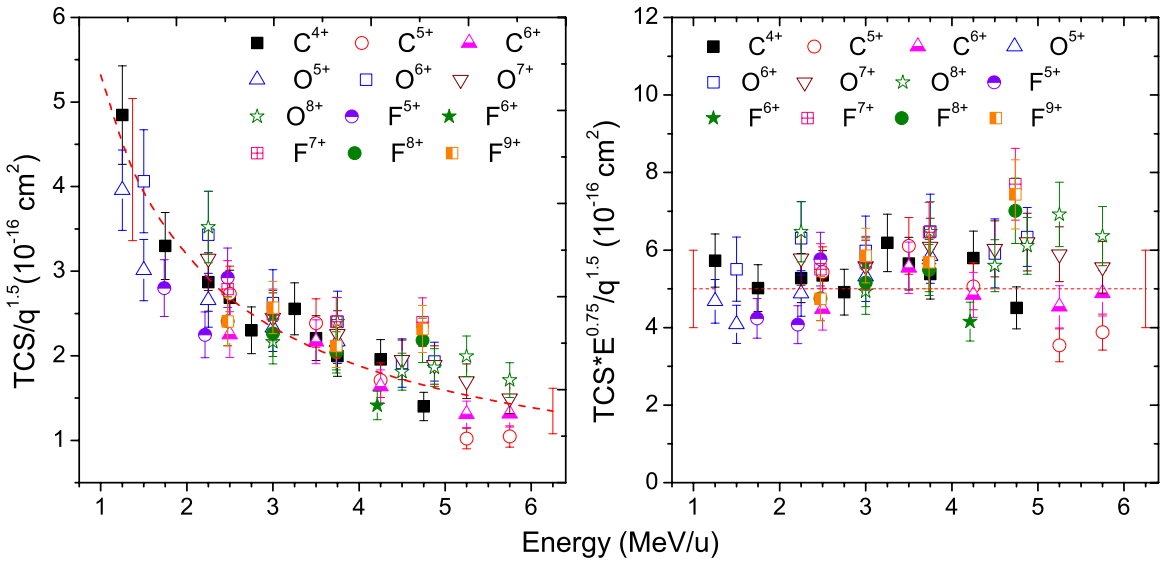

Figure 6. Scaling of the TCS obtained for the C, O and F projectiles with (a) projectile charge state q and (b) projectile energy E.

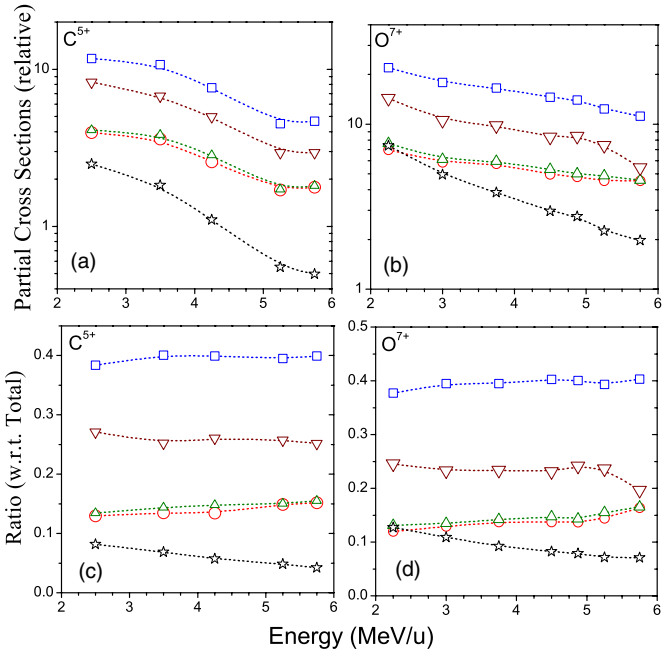

Figure 7. Partial cross sections of fragments of uracil in collisions with (a) C^{5+}, (b) O^{7+} ions. Parts (c) and (d) show the ratio of fragments with regards to the total ionization for C^{5+} and O^{7+} respectively. The symbols ◯, Δ, □, ▽, ⋆ represent mass 112 (Ur^+), 69, 42, 28 and proton respectively.

C^{5+} and O^{7+} in the high-energy range. The yield of mass 42 includes those of masses from 39 to 43. The yields of all the fragments (figures 7(a) and (b)) show a sharp fall with the projectile energy. The yield of H^+ decreases more rapidly as compared to the other fragments.

The ratio of fragment yields to the total ionization yields are also plotted. In the high-energy range (figures 7(c) and (d)), the ratios do not seem to have any significant projectile energy dependence. The ratios do not change much with the projectile-ion charge state (except for H^+) and have similar values for the C^{5+} (figure 7(c)) and O^{7+} (figure 7(d)) ions. This trend has also been reported for other smaller molecules, such as CO and CH_4 [49, 50].

4. Conclusions

The absolute total ionization cross sections are measured for fast highly charged C, O and F ion impact on uracil. The charge state dependence of the TCS has also been investigated for all the energies. The cross sections are shown to fall sharply with the projectile energy. The fall in the cross sections is reproduced by the model calculations based on the CDW–EIS and CB1 approximations and CTMC–COB model. CTMC–COB provides better agreement with the data for most of the cases than the other two models reported. The quantum mechanical models (CDW–EIS and CB1) are about a factor of two and three higher than the data, respectively, for both the C and O ions. The deviations are even larger for F ions which may require further investigation. In all cases the deviation seems to increase at lower energies. We have also demonstrated the deviation from a q^2-dependence of the TCS expected from the first-order theories of ion–atom collisions. In addition, all the measured TCS data are shown to vary approximately as $(q/v)^{3/2}$. The absolute TCS, the energy distribution, deviation from q^2-dependence and finally a simple scaling procedure may provide useful inputs for modelling the radiation damage by heavy ions.

Acknowledgments

Authors acknowledge the Pelletron accelerator team for the smooth running of the machine.

Appendix. Normalization procedure

The doubly differential cross sections (DDCS) of the electron emission from uracil in collisions with 42 MeV C^{6+} ions were measured using an electron spectroscopy setup having an

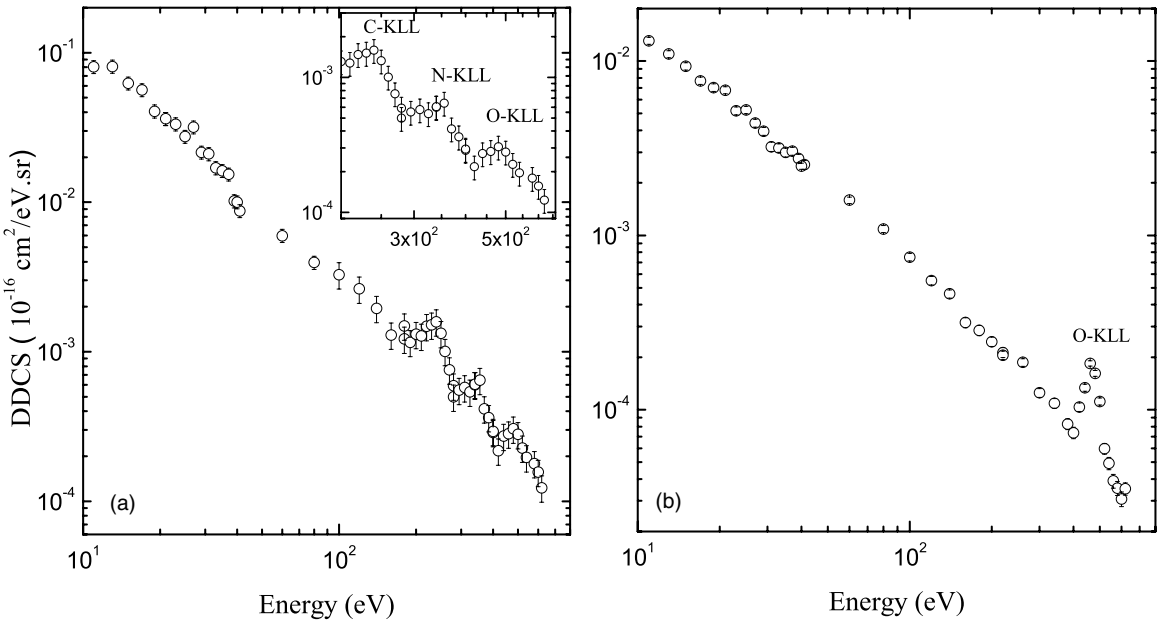

Figure A1. DDCS spectrum of (a) uracil and (b) O_2 in collisions with 42 MeV C^{6+} ions at $\theta = 30^\circ$. θ is the angle of emission of the electron with respect to incident beam direction.

electrostatic hemispherical analyser [51]. The measurements were carried out in the electron energy range of 10–620 eV and in an angular range of 30°–135°. The typical DDCS spectrum for uracil is shown in figure A1(a) which contains the Auger peaks of C, N and O atoms present in the molecule. The total cross sections (relative) ($\sigma_{\rm rel}^{\rm O-KLL}$) for the oxygen K-LL Auger electron from uracil were obtained by integrating the Auger peak over the electron energy and the emission angles.

Then the absolute electron DDCS were measured for the O_2 gas in a static gas condition using first principles. A typical DDCS spectrum is shown in figure A1(b). The total cross section (TCS) for oxygen K-LL Auger electrons from O_2-molecules ($\sigma_{\rm abs}^{\rm O-KLL}$) were obtained by integrating the e-DDCS over the Auger peak and entire angular range.

Assuming that the inner-shell ionization cross section of oxygen is the same in the case of uracil or the O_2 molecule as targets, a normalization factor was obtained by comparing the oxygen K-LL cross sections for these two targets. The normalization factor thus obtained was used to normalize the continuum part of the e-DDCS spectrum obtained for uracil [52]. Now, integrating the absolute DDCS spectrum of uracil over the entire energy and the emission angles provides the absolute TCS ($\sigma_{\rm abs}$) of uracil ionization for the 42 MeV C^{6+} ions. The error due to lack of measurements at extreme forward (<30°) and backward angles (>135°) was estimated to be ∼5%. The total error due to the normalization procedure was estimated to be ∼20%.

References

[1] McDowell M R C and Coleman J P 1970 *Introduction to the Theory of Ion–Atom Collisions* (Amsterdam: North-Holland) p 373 chapter 8
[2] Lee D H *et al* 1990 *Phys. Rev.* A **41** 4816
[3] Fainstein P D, Ponce V H and Rivarola R D 1991 *J. Phys. B: At. Mol. Opt. Phys.* **24** 3091
[4] Fainstein P D, Gulyas L, Martin F and Salin A 1996 *Phys. Rev.* A **53** 3243
[5] Suárez S, Garibotti C, Meckbach W and Bernardi G 1993 *Phys. Rev. Lett.* **70** 418
[6] Stolterfoht N *et al* 1995 *Phys. Rev.* A **52** 3796
[7] Tribedi L C *et al* 1996 *Phys. Rev. Lett.* **77** 3767
[8] Misra D *et al* 2007 *Phys. Rev.* A **75** 052712
[9] Friedland W, Dingfelder M, Kundrát P and Jacob P 2011 *Mutat. Res.* **711** 28
[10] Bernal M A, de Almeida C E, Sampaio C, Incerti S, Champion C and Nieminen P 2011 *Med. Phys.* **38** 4147
[11] Coupier B *et al* 2002 *Eur. Phys. J.* D **20** 459
[12] Moretto-Capelle P and Le Padellec A 2006 *Phys. Rev.* A **74** 062705
[13] Iriki Y, Kikuchi Y, Imai M and Itoh A 2011 *Phys. Rev.* A **84** 032704
[14] Tabet J, Eden S, Feil S, Abdoul-Carime H, Farizon B, Farizon M, Ouaskit S and Mark T D 2010 *Phys. Rev.* A **81** 012711
[15] Agnihotri A N *et al* 2012 *Phys. Rev.* A **85** 032711
[16] deVries J, Hoekstra R, Morgenstern R and Schlatholter T 2003 *Phys. Rev. Lett.* **91** 053401
[17] Brédy R *et al* 2007 *Nucl. Instrum. Methods* B **261** 114
[18] Imhoff M, Deng Z and Huels M A 2005 *Int. J. Mass Spectrom.* **245** 68
[19] Bernard J, Bredy R, Chen L, Martin S and Wei B 2006 *Nucl. Instrum. Methods Phys. Res.* B **245** 103
[20] Schlatholter T *et al* 2006 *Chem. Phys. Chem.* **7** 2339
[21] Alvarado F, Bari S, Hoekstra R and Schlatholter T 2006 *Phys. Chem. Chem. Phys.* **8** 1922
[22] Bacchus-Montabonel M C, Labuda M, Tergiman Y S and Sienkiewicz J E 2005 *Phys. Rev.* A **72** 052706
[23] Abbas I *et al* 2008 *Phys. Med. Biol.* **53** N41
[24] Lekadir H *et al* 2009 *Phys. Rev.* A **79** 062710
[25] Dal Cappello C, Hervieux P A, Charpentier I and Ruiz-Lopez F 2008 *Phys. Rev.* A **78** 042702
[26] Champion C *et al* 2010 *Phys. Med. Biol.* **55** 6053
[27] Galassi M E *et al* 2012 *Phys. Med. Biol.* **57** 2081
[28] Champion C *et al* 2012 *Phys. Med. Biol.* **57** 3039
[29] Fainstein P D, Ponce V H and Rivarola R D 1988 *J. Phys. B: At. Mol. Opt. Phys.* **21** 287

[30] Galassi M E, Rivarola R D and Fainstein P D 2004 *Phys. Rev.* A **70** 032721
[31] Belkic Dž, Gayet R and Salin A 1979 *Phys. Rep.* **56** 279
[32] Frisch M J *et al* 2009 Gaussian 09, Revision A.02 (Wallingford, CT: Gaussian Inc.)
[33] INFICON SQM 160 Multi-Film Rate/Thickness monitor
[34] Jochims H-W, Schwell M, Baumgartel H and Leach S 2005 *Chem. Phys.* **314** 263
[35] Schlathlter T, Hoekstra R and Morgenstern R 2004 *Int. J. Mass Spectrom.* **233** 173
[36] Denifl S *et al* 2004 *Int. J. Mass Spectrom.* **238** 47
[37] Imhoff M, Deng Z and Huels M A 2007 *Int. J. Mass Spectrom.* **262** 154
[38] NIST Chemistry web book http://webbook.nist.gov
[39] Heber O, Sampoll G, Bandong B B, Maurer R J, Watson R L, Ben-Itzhak I, Sanders J M, Shinpaugh J L and Richard P 1995 *Phys. Rev.* A **52** 4578
[40] Mergel V, Dorner R, Khayyat Kh, Achler M, Weber T, Jagutzki O, Ludde H J, Cocke C L and Schmidt-Bocking H 2001 *Phys. Rev. Lett.* **86** 2257
[41] Feil S, Gluch K, Matt-Leubner S, Scheier P, Limtrakul J, Probst M, Deutsch H, Becker K, Stamatovic A and Märk T D 2004 *J. Phys. B: At. Mol. Opt. Phys.* **37** 3013
[42] Olson R E, Berkner K H, Graham W G, Pyle R V, Schlachter A S and Stearns J W 1978 *Phys. Rev. Lett.* **41** 163
[43] Madison D H and Merzbacher E 1977 *Atomic and Inner Shell Processes* ed B Crasemann (New York: Academic) pp 1–72
[44] Kelkar A H, Kadhane U, Misra D, Gulyás L and Tribedi L C 2010 *Phys. Rev.* A **82** 043201
[45] Kadhane U, Kelkar A, Misra D, Kumar A and Tribedi L C 2007 *Phys. Rev.* A **75** 041201
[46] Datz S *et al* 1990 *Phys. Rev.* A **41** 3559
[47] Haugen H K, Andersen L H, Hvelplund P and Knudsen H 1982 *Phys. Rev.* A **26** 1950
[48] Ben-Itzhak I, Gray T J, Legg J C and McGoire J H 1988 *Phys. Rev.* A **37** 3685
[49] Krishnamurthi V, Ben-Itzhak I and Carnes K D 1996 *J. Phys. B: At. Mol. Opt. Phys.* **29** 287
[50] Malhi N B, Ben-Itzhak I, Gray T J, Legg J C, Needham V, Carnes K and McGuire J H 1987 *J. Chem. Phys.* **87** 6502
[51] Misra D, Thulasiram K V, Fernandes W, Kelkar A H, Kadhane U, Kumar A, Singh Y, Gulyás L and Tribedi L C 2009 *Nucl. Instrum. Methods Phys. Res.* B **267** 157
[52] Agnihotri A N *et al* 2013 *Phys. Rev.* A **87** 032716